Temperature effects on the global patterns of photosynthetic quantum efficiency

David Sandoval[1], Victor Flo[1,2], Catherine Morfopoulos[1,3] and Iain Colin Prentice[1,4,5]

[1]Georgina Mace Centre for the Living Planet, Department of Life Sciences, Imperial College London, Ascot, UK
[2]Univ Autònoma de Barcelona, Cerdanyola del Vallès 08193, Spain
[3]Department of Geoscience, Environment & Society-BGEOSYS, Université Libre de Bruxelles, Brussels, Belgium
[4]Department of Biological Sciences, Macquarie University, North Ryde, Australia
[5]Department of Earth System Science, Tsinghua University, Beijing, China

Abstract

The photosynthetic quantum efficiency (φ_0) is a key input parameter for modelling gross primary productivity in terrestrial biosphere models. Historically, these models assumed φ_0 to be constant, based on leaf measurements under unstressed conditions and within a narrow temperature range. However, increasing evidence suggests a temperature-dependent φ_0 on temperature, though it remains unclear whether this response is generalized or if it propagates to the ecosystem. Here, we derived $\varphi_0(T)$ at the ecosystem level for sites distributed globally, using sub-daily eddy covariance measurements of CO_2 exchange and above/below-canopy measurements of photosynthetic flux density to derive the fraction of absorbed photosynthetically active radiation (fAPAR). We found that $\varphi_0(T)$ shows a consistent bell-shaped response curve with temperature in all the sites we analysed. These patterns held when analysed with a larger global dataset using remotely sensed fAPAR. Furthermore, we observed that the values of $\varphi_0(T)$ are not markedly different among biomes, instead, there is a gradual transition of the peak $\varphi_0(T)$ which decreases following an aridity gradient. Additionally, we noted varying sensitivity to temperature among the different sites, with sensitivity increasing as growth temperature decreases.

Introduction

Photosynthesis is the major process driving life on Earth. Given its synergy and feedback with the terrestrial carbon cycle, uncertainties in its prediction can cause huge discrepancies when we project ecosystem responses to global environmental change [1]. Our current understanding of this process is enclosed in the representations of photosynthesis within terrestrial biosphere models (TBMs). These representations are based on biochemical models, which typically rely on similar implementations of the Farquhar, von Caemmerer and Berry (FvCB) model [1]. Such implementations use different assumptions, conceptualizations of the in-canopy processes and parameterizations, but share the same core equations [2]. Thus, in theory, they should yield gross primary productivity (GPP) predictions with only minor divergence, however, the actual discrepancies are worrisome [1,3,4]. One of the major causes for such discrepancies in these predictions is the value adopted for one of the key input parameters: photosynthetic quantum efficiency or intrinsic quantum yield (φ_0). This parameter represents the initial slope of the photosynthesis' light response curve under non-photorespiratory conditions (i.e., high CO_2 and/or low O_2 partial pressures), thus, it defines the maximum efficiency of photosynthesis [2,5].

Although extensive research has been done since the maximum possible value for φ_0 was established in the 1950's as one mole of assimilated CO_2 per eight moles of absorbed photons [6–9], almost all values reported in the literature since then were obtained from measurements in leaves. These measurements were conducted under a forced non-photorespiratory atmosphere, within a narrow temperature range of 25~30 ºC and with well irrigated plants. Under these specific conditions φ_0 falls within the range of 0.07~0.125 mol CO_2 mol^{-1} photon, with higher values observed in shade-adapted plants and lower in C4 compared to C3 plants [5,10–14].

Despite the limited knowledge of how φ_0 responds to temperature and water availability, and how it propagates from leaves to the ecosystem, it was assumed that the available leaf-level observations were representative and sufficient to infer a single global value[5,9,13]. This assumption led to TBMs adopting values of φ_0 close to 1/8 and independent of temperature[2]. In contrast to this view of a unique φ_0, fully empirical models of light use efficiency (LUE) that incorporate a downward regulation factor for CO_2 (e.g., Zhang et al.[15]; Bao et al.[16]; Pei et al.[17]) rely on different prescribed values of LUE_{max} (equivalent to φ_0) per plant functional type, rivalling the performance of TBMs.

The temperature independence of φ_0 can be theoretically examined using a corollary to the FvCB theory [18,19], which can approximate the maximum efficiency of photosynthesis under

ambient atmospheric conditions (φ) as:

$$\varphi \approx \lim_{I \to 0} \frac{\partial A}{\partial I} = \frac{c_i - \Gamma^*}{8c_i + 16\Gamma^*}(1-f)\alpha = \frac{1}{8}\, m_j (1-f)\alpha \qquad (1)$$

where A is carbon assimilation, I is the incident irradiance, c_i the intercellular CO_2 partial pressure, α the leaf absorptance, and f is defined as a correction factor for light quality assumed as 0.15 [19]. Here, the photorespiratory compensation point Γ^* is defined as:

$$\Gamma^* = \frac{pO_2\, K_c\, V_{omax}}{2K_o\, V_{cmax}} \qquad (2)$$

were pO2 is the partial pressure of oxygen, V_{max} the maximum rate, and K the Michaelis–Menten coefficients (temperature dependent), the subscripts $_o$ and $_c$ refer to oxygenation and carboxylation respectively.

This corollary predicts that under non-photorespiratory conditions the effect of Γ^* and its temperature dependency will be at a minimum. Thus m_j will approach to 1.0, hence φ will be close to $\frac{1}{8}\,(1-f)\alpha$ independently of the temperature. While under photorespiratory conditions (ambient CO_2 and O_2) φ would decline with temperature due to the greater temperature sensitivity of Ko than Kc. Both predictions of this theory are inconsistent with empirical models, φ is overestimated at low temperature under both non-photorespiratory and ambient CO_2 conditions (Fig. 1). As noted by Rogers et al.[20] on arctic plants, the predicted change of φ with temperature was opposite to what was observed, matching the predictions only at 25ºC. These results may explain the inconsistencies in temperature responses of GPP predicted by models [21], suggesting the need for an explicit correction for $\varphi_0 = f(T)$ when using a FvCB type model.

Few studies have investigated the effect of temperature on quantum efficiency, with most focusing on the quantum efficiency of photosystem II (ϕ_{PSII}), which is proportional to φ_0 [12,22]. When this quantity is measured using chlorophyll fluorescence on dark-adapted leaves there is no noticeable effect of temperature, in light adapted leaves, on the other hand ϕ_{PSII} shows a distinctive response to temperature [23]. Here, some researchers agree on a hump-shaped temperature response [23–25], but with inconsistencies in their peaks and inflection points (Fig. 1a). In contrast, others report only an increase [26] (Fig. 1a). The inconsistencies are even more pronounced for φ. Presumably, in this case, the authors were observing different regions of

the temperature range, reporting either increases [20,27] or decreases [28] in the responses (Fig. 1b). The strong differences in these quantum efficiency responses to temperature underline the need for a global approach at the ecosystem level.

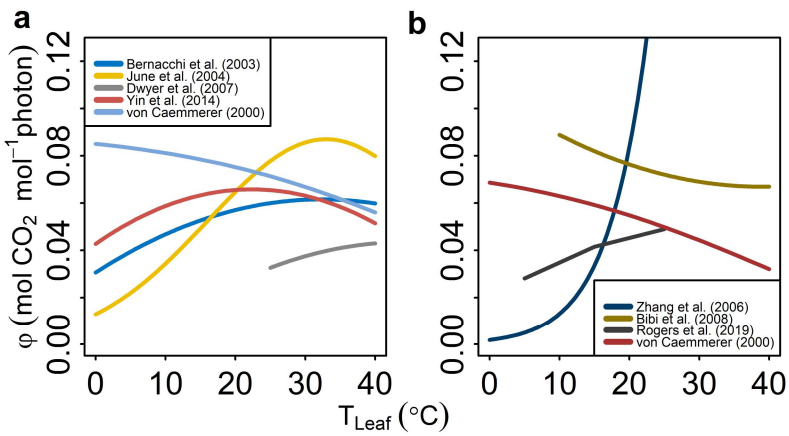

Figure 1. Quantum efficiency response to temperature observed by several authors upscaled to average peak of 0.087 molCO_2 mol^{-1}photon. **a** non-photorespiratory conditions, Eq. (1) forced here with CO_2 = 750 ppm. **b** ambient atmospheric conditions Eq. (1) forced here with CO_2 = 400 ppm.

In this study we leverage the great amount of subdaily data from eddy covariance carbon flux measurements, plus in situ observations of the fraction of absorbed photosynthetic active radiation (fAPAR) from the Ameriflux network (AMF) [29]. For each site and 1 °C temperature intervals, we estimated φ_0 by fitting a rectangular hyperbola to the upper envelope points of the light-assimilation space. We corrected φ_0 for photorespiratory conditions and vapour pressure deficit (D) affecting stomatal closure, by inverting a photosynthesis model based on eco-evolutionary optimality principles (EEO) [30,31] (see Methods). Then, we evaluated the shape of $\varphi_0 = f(T)$ using φ_0 from each temperature bin vs. the centre value of the same bin. We replicated the analysis with a larger set of sites from the Fluxnet network (FLX) [32] using fAPAR from remote sensing [33].

We hypothesized that if the peak-type response of φ_0 to temperature observed at leaf level (Fig. 1a) is indeed a generalized plant response it should propagate to the ecosystem and it should emerge globally. Additionally, we also hypothesized that if the shape of $\varphi_0 = f(T)$ changes across sites, the parameters shaping these response curves might correlate with the sites' bioclimatic metrics such as aridity (AI) or growth temperature ($mGDD_0$). We used peaked-Arrhenius (PA) curves to propose some interpretation to this bioclimatic effect.

Results

We found a large variability of φ_0 across all biomes and climate zones. Both datasets exhibited similar patterns within biomes, with the exception of savannas (SAV) and wetlands (WET), which showed considerably lower values in the AMF dataset compared to their counter parts in the FLX dataset. The average estimates of φ_0 varied among biomes but exhibited a smooth transition: high values shown by forests were followed by lower values in grasslands and shrublands (Fig. 2a). When we examined this transition using climate zones a marked pattern emerged driven by an aridity gradient. Here, tropical rainforest (Af) and tropical monsoon (Am) sites appeared at the upper end of the φ_0 axis, followed by sites with "no dry season" (*f* types), and then by sites with dry/wet seasonality (*w* and *s* types). Finally, sites from arid climates (BW*) and steppe appeared in the lower end (BS*) (Fig. 2b and 2c).

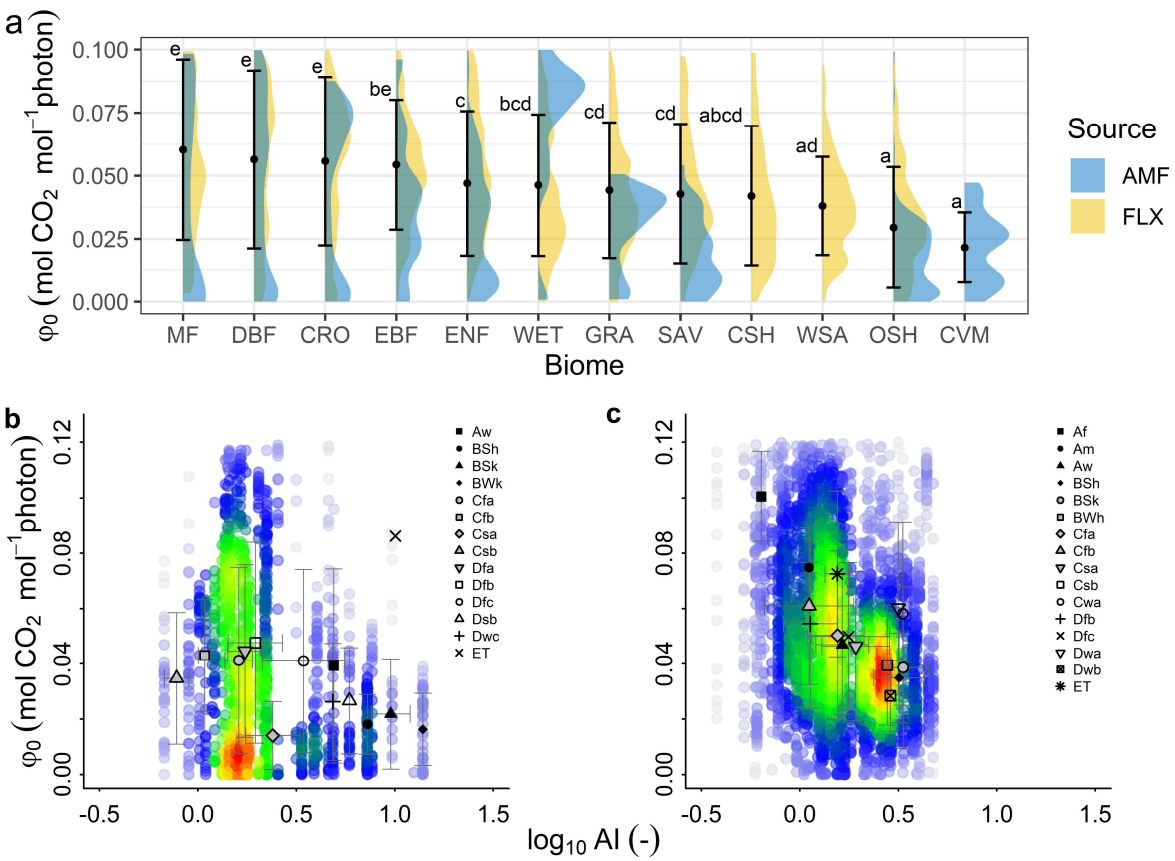

Figure 2. Observed φ_0 at AMF and FLX sites. **a** Probability distribution of φ_0 per biome and fAPAR source. The dot and the black bar denote the mean and SD of the combined sources per biome, respectively. Post hoc Tukey test results at the top of the bars. **b** φ_0 as a function of aridity index from Ameriflux sites. **c** φ_0 as a function of aridity index from Fluxnet sites. Symbols in panels **b** and **c** show the average φ_0 values per climate zone.

As we expected, the variation of φ_0 with temperature exhibited a hump-shaped pattern across all sites (Fig. 3a). In general, the average φ_0 steadily increased up to a maximum, followed by a sharp drop. This pattern also emerged using the 75th and 95th percentiles of φ_0 (Fig. 3a). Both datasets displayed similar values of φ_0 at the optimal temperature of 20.35 ± 0.33 ºC. The global maximum efficiency found within the 95th percentile was 0.111 ± 0.003 mol CO_2 mol^{-1} photon. When we examined the shape of these relationships at the biome level, we found that the hump-shaped response remained consistent (Fig 3b). On average, OSH exhibited lower φ_0 values and lower sensitivity to T_{air}, whereas MF showed the highest φ_0 values and higher sensitivity to T_{air}. In biomes where the same temperature range was recorded by both datasets (i.e., DBF, MF and OSH) the sensitivity $\varphi_0(T)$ showed very similar patterns between datasets. Whereas in ENF, GRA and EBF biomes, interestingly, the FLX dataset showed higher φ_0 at low temperatures which may be attributed to potential underestimations of the satellite-derived fAPAR values under these conditions. In biomes where the recorded temperature covered a narrower range, the peaks were higher (i.e., EBF and WET).

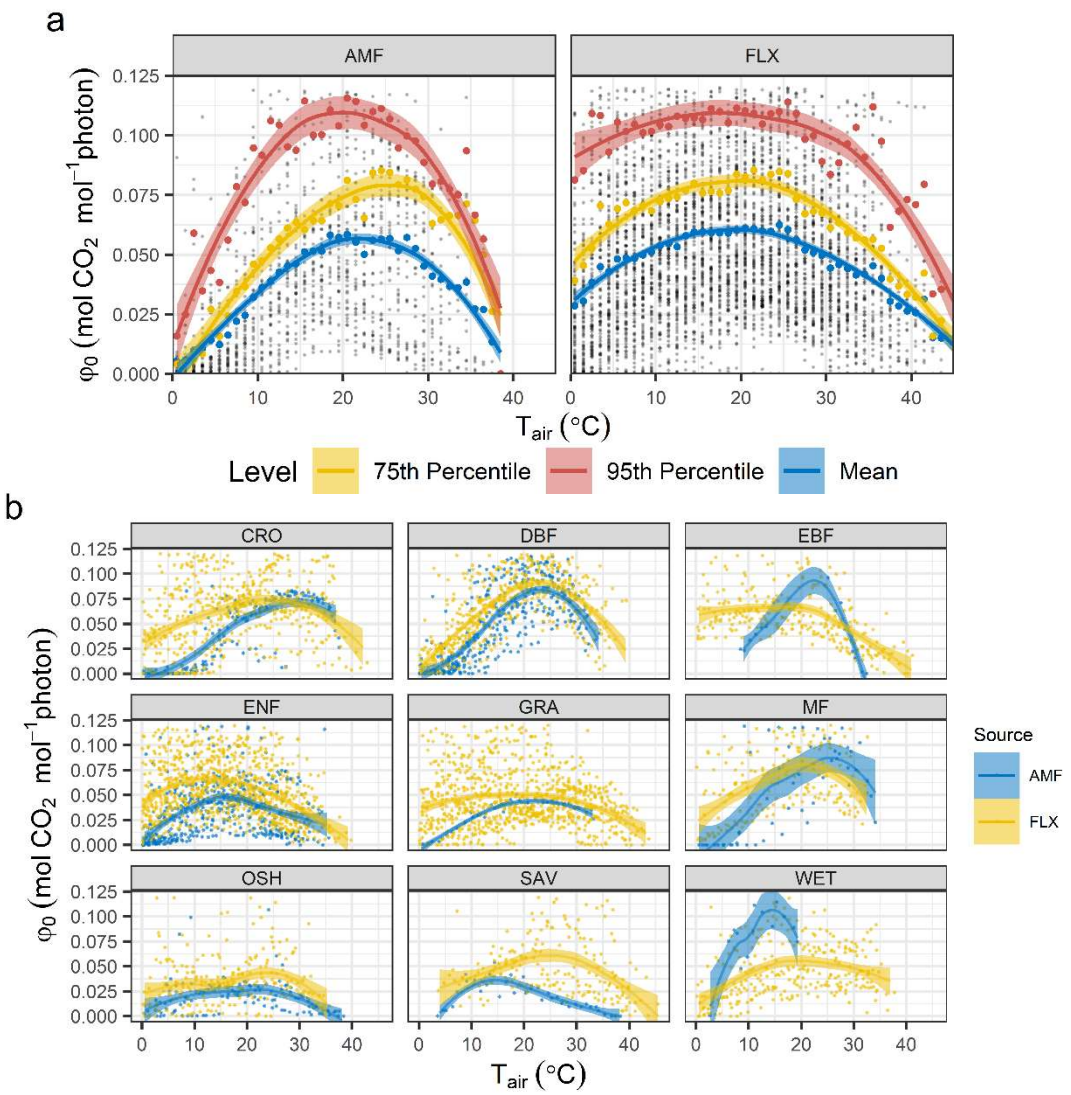

Figure 3. φ_0 response to temperature using all the data pooled, the ribbons shows a LOESS smoothing function including its 95% confidence intervals (a) Observations from AMF sites with in situ fAPAR. and FLX sites with RS fAPAR. (c) Observations per biome and dataset.

The curves fitted per site to the PA equation were able to explain $\varphi_0(T)$ with reasonably good accuracy. Here the PA curves performed better for the AMF dataset, explaining 81% of the variation, while most of the mean values, observed and simulated per biome fell into the 1:1 line, except for OSH which was slightly overestimated (Fig. 4a). For the FLX dataset, the fitted PA curves explained 65% of the variation, overestimating the mean values per biome (Fig. 4b). The φ_0 at the peak (pre-exponential factor) showed high variation among sites (Fig. 4c), while the ativation energy was relatively stable. The activation energy did not show much variation among sites. For most of them (~230 sites) it reached ~75 kJ mol^{-1}. On the other hand, the activation entropy varied from ~150 J mol^{-1} K^{-1} to >1200 J mol^{-1} K^{-1}. The deactivation energy was highly correlated with the activation entropy. The latest also exhibit great variation among sites.

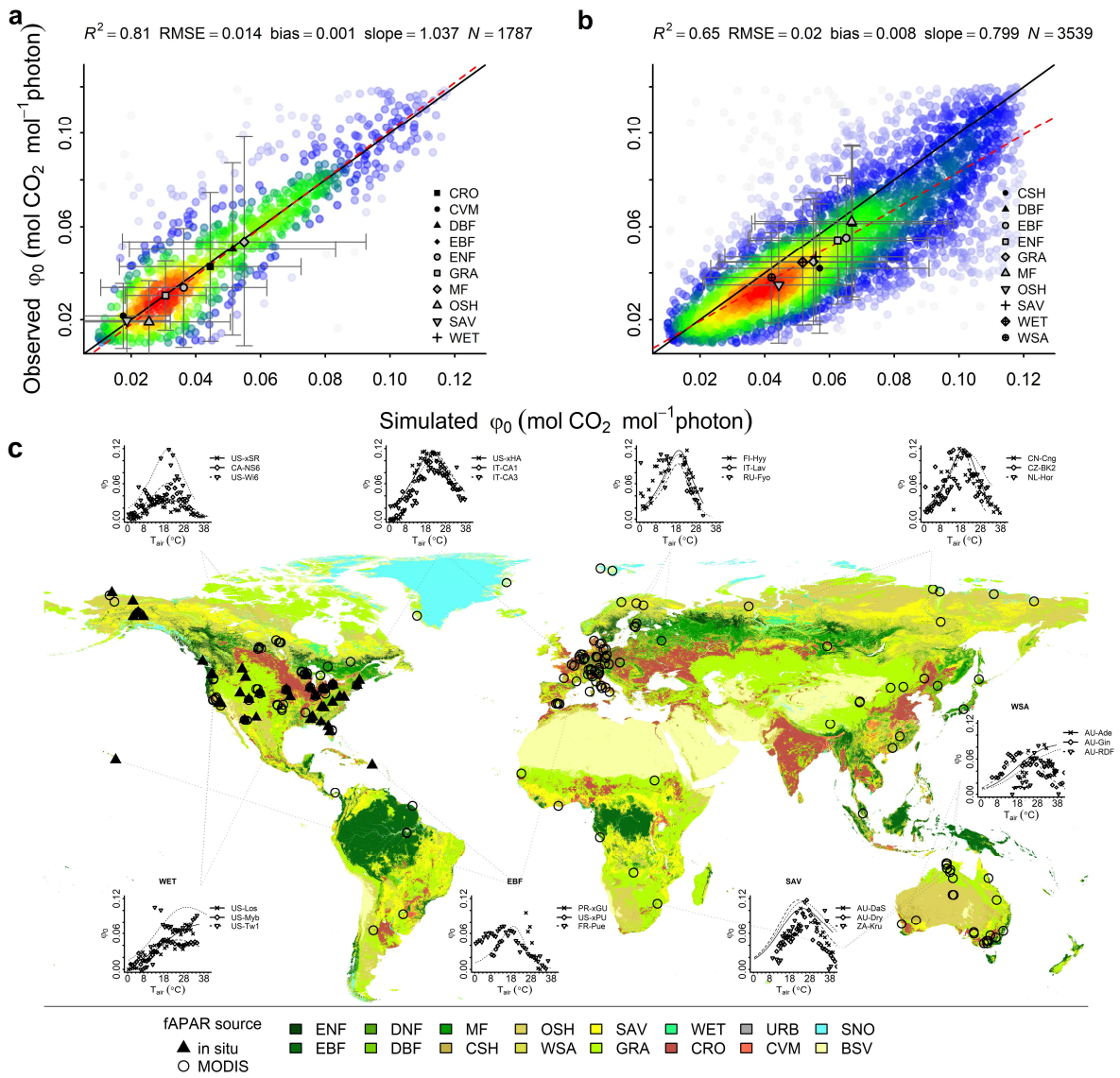

Figure 4. φ_0 response to temperature modelled using peaked-Arrhenius curves. **a** Correlation of observed and simulated φ_0 using in situ fAPAR. **b** Correlation of observed and simulated φ_0 using RS fAPAR. **c** Observation (points) and predictions (lines) form selected sites around the globe.

The peak φ_0 ($\widehat{\varphi_0}$) decreased following an s-type response (eq. 3) from a plateau of 0.111 <= 1, followed by a steep decay from AI>1 to AI≈4, with a value around 0.02 (Fig. 5a).

$$\widehat{\varphi_0} = \frac{0.111}{(1+AI^m)^n} \qquad (3)$$

This wet-dry transition also emerges when $\widehat{\varphi_0}$ is plotted against evaporative fraction (EF) (annual mean of actual over potential evapotranspiration). Here $\widehat{\varphi_0}$ increases linearly with EF until it reaches a plateau at around EF≈0.6. Sites that outside the 95% confidence intervals are tagged in the plots and discussed in the next section. The global average of $\widehat{\varphi_0}$, according to the prediction from equation (3) was 0.08. ΔS decreases linearly from 1306.88 J mol^{-1} K^{-1} at mGDD$_0$ = 5 ºC with a slope of 50.223 K^{-1}. The T_{opt} predicted by equation (4) follows mGDD$_0$ up to ~20 ºC when it increases exponentially.

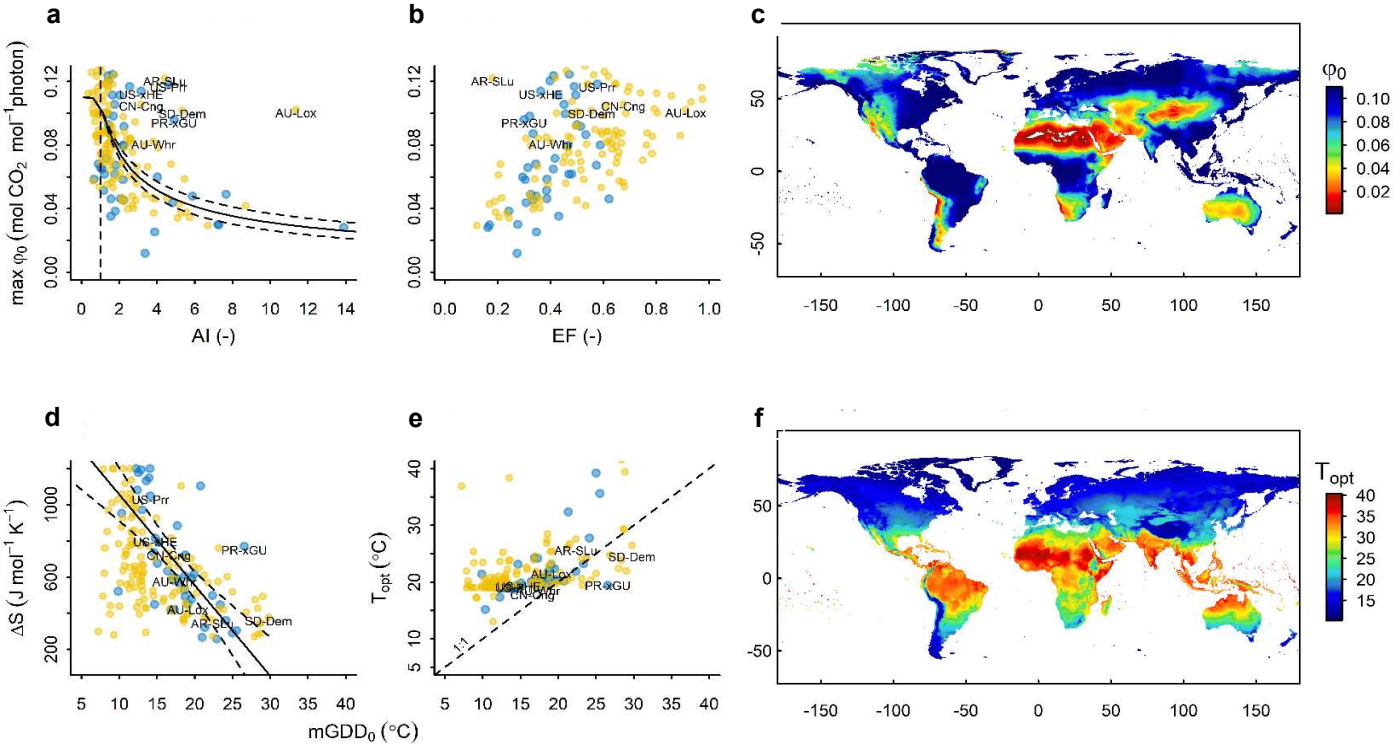

Figure 5. Bioclimatic patterns of the Arrhenius parameters, the colors in the scatter plots refers to AMF and FLX datasets as in Fig 1a. **a** $\widehat{\varphi_0}$ response to aridity, solid line regression, dashed lines 95% confidence intervals. **b** $\widehat{\varphi_0}$ response to Evaporative fraction. **c** Global prediction of $\widehat{\varphi_0}$ using equation (3). **d** Activation entropy response to growth temperature, solid line regression, dashed lines 95% confidence intervals. **e** Correlation of the optimum temperature predicted by Arrhenius and growth temperature. **f** Global prediction of optimum temperature for $\varphi_0(T)$ using equation (8).

Discussion

We derived φ_0 at the ecosystem level for globally distributed sites, using sub-daily in situ measurements of fAPAR and eddy covariance measurements of CO_2 exchange. We found that φ_0 shows a bell-shaped response with temperature at ecosystem level and that this shape remains consistent across all the sites we analysed, even when remotely sensed fAPAR was used. Additionally, we observed that φ_0 is not unique among biomes, but instead, there is a gradual transition of $\widehat{\varphi_0}$ which decreases along an aridity gradient. Furthermore, we found different temperature sensitivities at each site, with sensitivity increasing as $mGGD_0$ decreases.

The observed variation of $\varphi_0(T)$ among biomes, suggests that $\varphi_0(T)$ could also vary among species, contrary to what has been suggested by Björkman & Demmig[12]; Walker[9]; Long et al. [5]. Since we corrected for photorespiration and stomatal closure, the observed variation of φ_0 was primarily due to aridity and temperature, in line with Singsaas et al.[13] who noted that even a variation of 100% in photorespiration plus alternative electron sinks could not account for the observed variation in φ_0 among species. Although according to Eq. (6) R_d offsets the LRC in each temperature bin without affecting φ_0, we double-checked our results by repeating the analysis using GPP from the FLX dataset and setting R_d=0.0, obtaining very similar results (Fig. A4).

The maximum observed value of φ_0 (mol CO_2 mol^{-1} photon) closely matches values reported as maximum efficiency under unstressed conditions by Björkman & Demmig[12]; (0.106), Skillman [14] (0.106) Walker[9] (0.111) and Singsaas et al.[13] (0.108). However, it is lower than the theoretical value of 0.125 from Emerson[6] and Singsaas et al.[13] but closer to what is estimated as the maximum efficiency limited by ATP generation (0.111) [5].

The pattern of $\varphi_0(T)$ observing across forests, grasslands and shrublands, is consistent with observations made by Björkman & Demmig[12] in species from these biomes, although the variation noted there was similar to the error limits of around 1%. This difference among biomes could be attributed to the enclosed and layered canopy structure of forests, which prevents leaves in the lower canopy from being exposed to excessive light that could cause photodamage and reduce φ_0 [34].

The results support our hypothesis on the bell-shaped response of φ_0 to temperature as a general plant response, which propagates to the ecosystem, thus creating a general ecosystem response to temperature. This emergent response is possibly depicting the kinetic

347 energy of chlorophyll molecules in their ground state and the vibrational excitation energy
348 provided by an increase in temperature [9]. Since we corrected for photorespiration, implicitly
349 accounting for rubisco deactivation at high temperature, this new function would imply a
350 sharper decline in assimilation under ambient atmospheric conditions when the temperature
351 is higher than T_{opt}.
352
353 Moreover, φ_0 reflects the combined efficiency of PSI and PSII which exhibit different
354 responses to temperature in light-adapted leaves. For example, it has been reported that PSI
355 activity decreases at low temperatures only in cold-sensitive plants [35], otherwise it remains
356 thermally stable. Its inactivation does not occur before the complete inactivation of PSII [36,37].
357 ϕ_{PSII}, on the other hand, shows a similar bell-shaped response to temperature, this response
358 is well documented in many studies (e.g., [23–25]).
359 (e.g., Bernacchi et al. [23]; June et al. [25]; Yin et al. [24]). Considering the linear relationship between
360 ϕ_{PSII} and φ_0 [12,22] it is very likely that this interdependence largely shapes the φ_0 response to
361 temperature. Moreover, the low φ_0 at low temperature could be explained by the rate of repair
362 of PSII, which slows down at low temperature [38,39]. If this rate of repair becomes slower than
363 the rate of PSII damage, it could lead to photoinhibition even at limiting low light [40,41]. This
364 damage-repair imbalance is also documented at high temperature, whereby the rate of
365 damage is enhanced by the increase in temperature [42,43].
366
367 With excess light, thermal dissipation of excess energy and non-photochemical quenching act
368 as photoprotective mechanisms diverting photons from photochemistry, thereby reducing the
369 quantum efficiency[37]. Conversely, at limiting light, fluorescence is the most likely dissipative
370 pathway of excess energy [44]. Thus, our results describing the temperature response of φ_0
371 suggest that the damage to the photosynthetic machinery due to temperature could accelerate
372 energy dissipative pathways even under low light, decreasing φ_0. Furthermore, φ_0 reflects the
373 efficiency of the entire electron transfer chain from H_2O to CO_2. This chain is mediated by the
374 cytochrome b_6f (Cyt b_6f) acting as a switch that redistributes excitation energy between
375 photosystems, thus modulating the coupling between cyclic and non-cycling electron flux and
376 diverting energy to thermal dissipation [45]. The maximum activity of Cyt b_6f depends on
377 temperature following a regular Arrhenius expression, while both the coupling efficiency of the
378 cyclic and non-cycling electron fluxes decay exponentially at high temperatures [45], therefore
379 φ_0 temperature response could be reflecting the emergent response of these processes.
380
381 Another factor that could be affecting $\varphi_0(T)$ is the solubility of CO_2 in water, which decreases
382 as temperature increases, reducing the CO_2 concentration in C3 plants and favouring

oxygenation by Rubisco, as observed by [10]. However, this effect is counterbalanced by the increase in CO_2 diffusivity and hence the increase on the mesophyll conductance [46].

Our results suggest that the maximum efficiency $\widehat{\varphi_0}$ decreases as climatological aridity increases, consistent with the observations of Fu et al.[47] regarding the maximum evaporative fraction and with Mengoli et al.[48] observing the maximum level of LUE. This pattern possibly reflects: 1. Persistent drought effects on the photosynthetic apparatus, such as the break of the light harvesting complexes of PSII and the reduction in the size of the PSI antenna [49]. 2. Drought-adapted traits, i.e., plants in dry regions would exhibit higher leaf mass per area (LMA) [50] constantly favouring photoprotective thermal dissipation over photochemistry [51,52]. Or 3. water use strategies, i.e., coordination of hydraulic and allocation traits [53], plant hydraulic risk tolerance and plant water flux control defining the minimum soil moisture limitation [54]. However, since many unknowns remain regarding the exact mechanisms that define how φ_0 propagates from leaf to the canopy and how vertical gradients in the canopy shape light exposure and, therefore, the adaptation of photosynthetic traits [55] these ideas still require further rigorous testing.

Some of the sites that didn't fall inside the confidence intervals of the equation (3) are irrigated sites like AU-Lox [56] or are tapping into the groundwater like SD-Dem [57].

The activation energy found with the peaked-Arrhenius curves did not exhibit much variation among sites, consistent with the values of Ea for V_{cmax} and J_{max} reported by Kattge & Knorr [58]. However, it contrasts with the reported variation with growth temperature by Kumarathunge et al.[59]. The activation entropy decreases with increasing $mGDD_0$, in line with the estimations of ΔS for V_{cmax} and J_{max} from Kattge & Knorr [58] and Kumarathunge et al.[59], possibly reflecting the effect of $mGDD_0$ on the chlorophyll ground state [37]. In our results, the variation in ΔS shifts the optimum temperature proportionally to $mGDD_0$ and simultaneously reduces the sensitivity of φ_0 to T. This response is consistent with the observations of increased thermal stability of PSII at higher growth temperatures due to changes in the thylakoid membrane lipids [37]. It is also consistent with the effect of higher growth temperatures on the accumulation of zeaxanthin, which enhances nonphotochemical quenching and thermal energy dissipation in PSII [44,60]. Overall, the variations of ΔS and $\widehat{\varphi_0}$ with mGDD0 and aridity respectively support our hypothesis about bioclimatic metrics shaping $\varphi_0(T)$.

We replicated our analysis on a year-by-year basis in sites with at least 10 years of in situ fAPAR records (n=3) (Fig A1), and we did not observe any signal of acclimation. While only 3

sites may not provide sufficient evidence to dismiss the possibility of $\varphi_0(T)$ acclimation, this observation is consistent with what was reported by [23], and would imply that the acclimation of the maximum rate of Rubisco activity (V_{cmax}) to temperature, which is a well-documented phenomenon [58,61] does not notably affect φ_0.

However, some studies do report acclimation to temperature of the initial slope of the light response curve, as seen in Dwyer et al.[26] in C4 grasses or Herrmann et al.[62] using a non-rectangular hyperbola. Here, this effect is attributed to the acclimation of the Θ shape parameter, not to φ_0. Nevertheless, if the equation from Smith [63] had been used here, the same fitting procedure would have resulted in φ_0 changing with the temperature. To our knowledge, only Tenhunen et al.[64] uses the same equation from Smith[63] as used here and finds a variation of φ_0 with temperature, but it is dropped to assume constant φ_0 for simplicity. Both equations are empirical, so further research is needed to properly trace the origin of this response.

This study provides, for first time, global evidence that φ_0 is not a fixed parameter as previously assumed in many TBMs, but instead exhibits a bell-shaped response to temperature. Moreover, we found that bioclimatic factors shape this response. In this way, the peak values respond to aridity, potentially defining the maximum LUE, while the sensitivity to temperature increases as growth temperature decreases. We proposed some ideas about possible causes of these responses, and we believe that incorporating these responses is key to assessing the thermal limits and tipping points of the terrestrial carbon sink, specially under future CO_2 emission scenarios.

Extended data

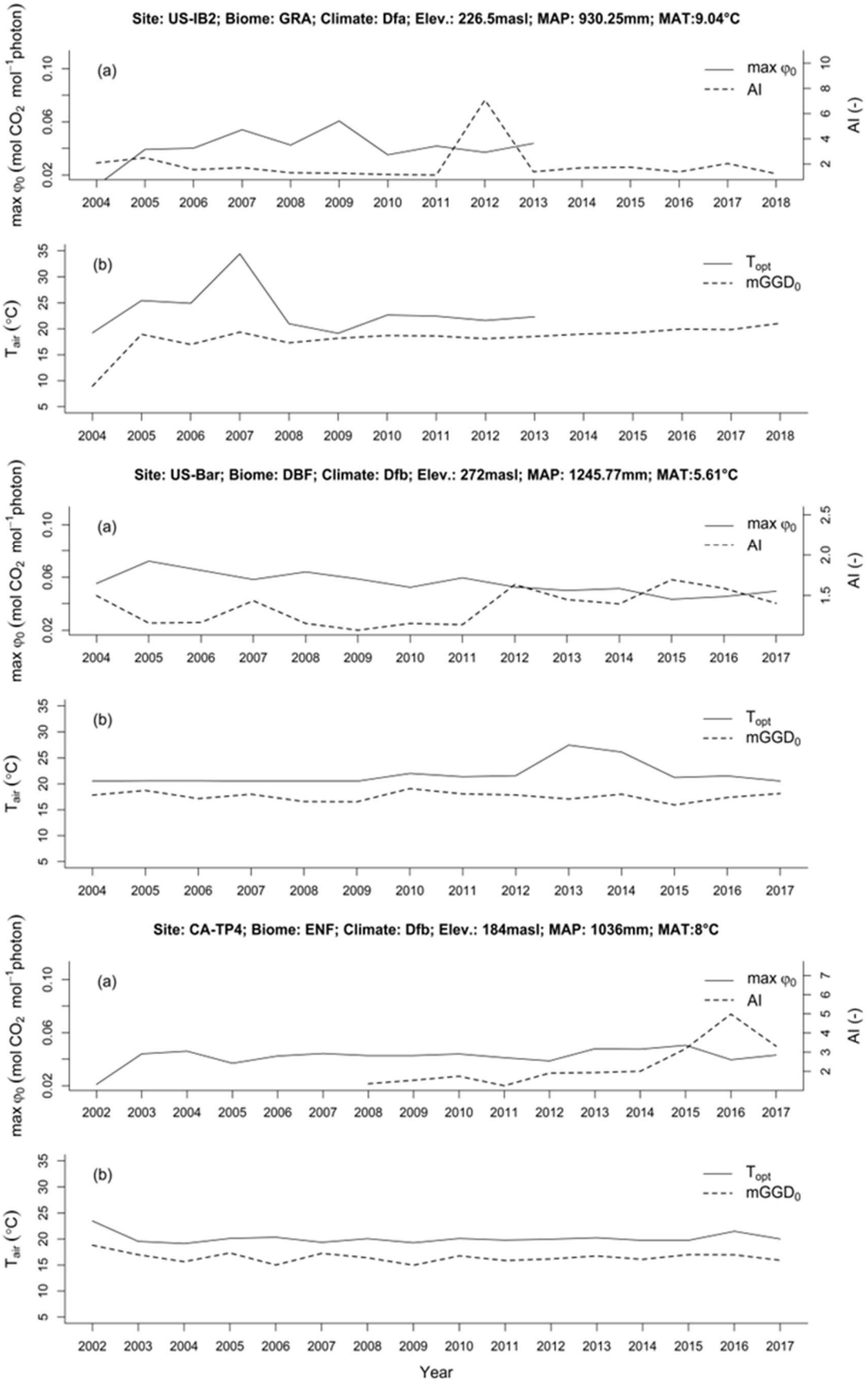

Figure A1. Temporal dynamics of the parameters shaping $\varphi_0(T)$ at a selected sites

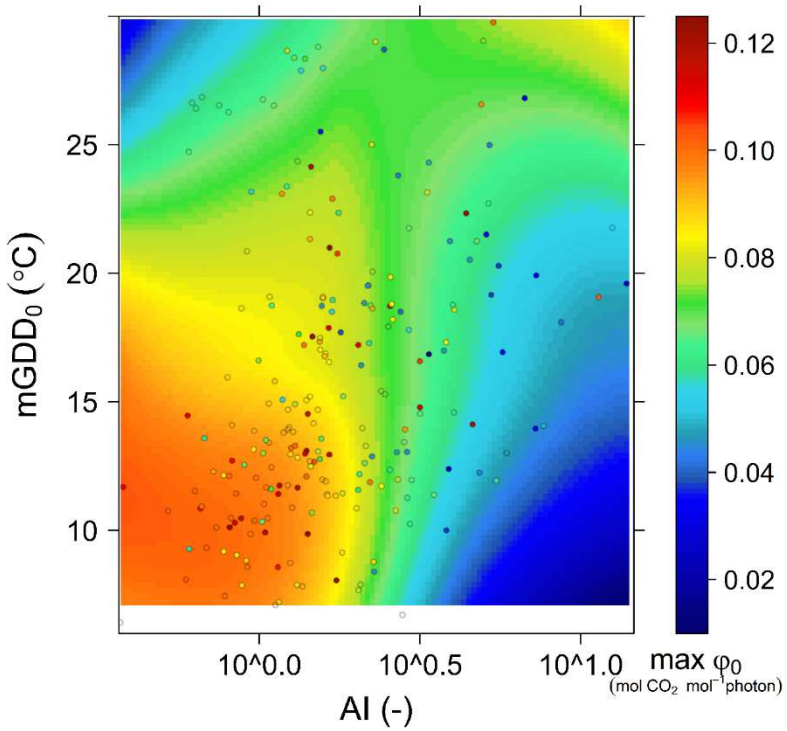

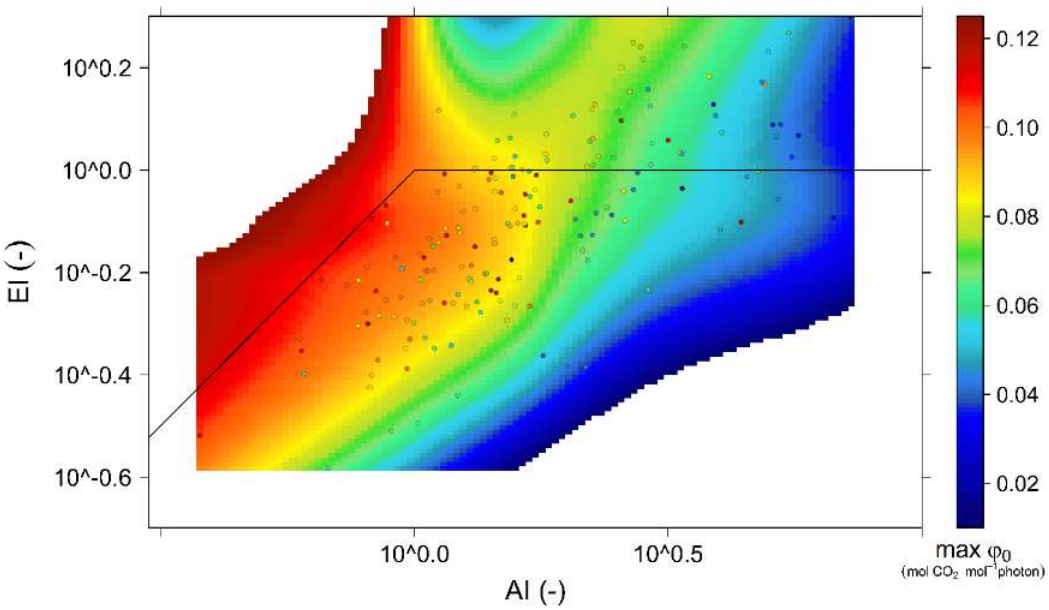

Figure A2. $\widehat{\varphi_0}$ depicted in climate spaces. (a) $\widehat{\varphi_0}$ in the space aridity-growth temeprature. (b) $\widehat{\varphi_0}$ in the Budyko space

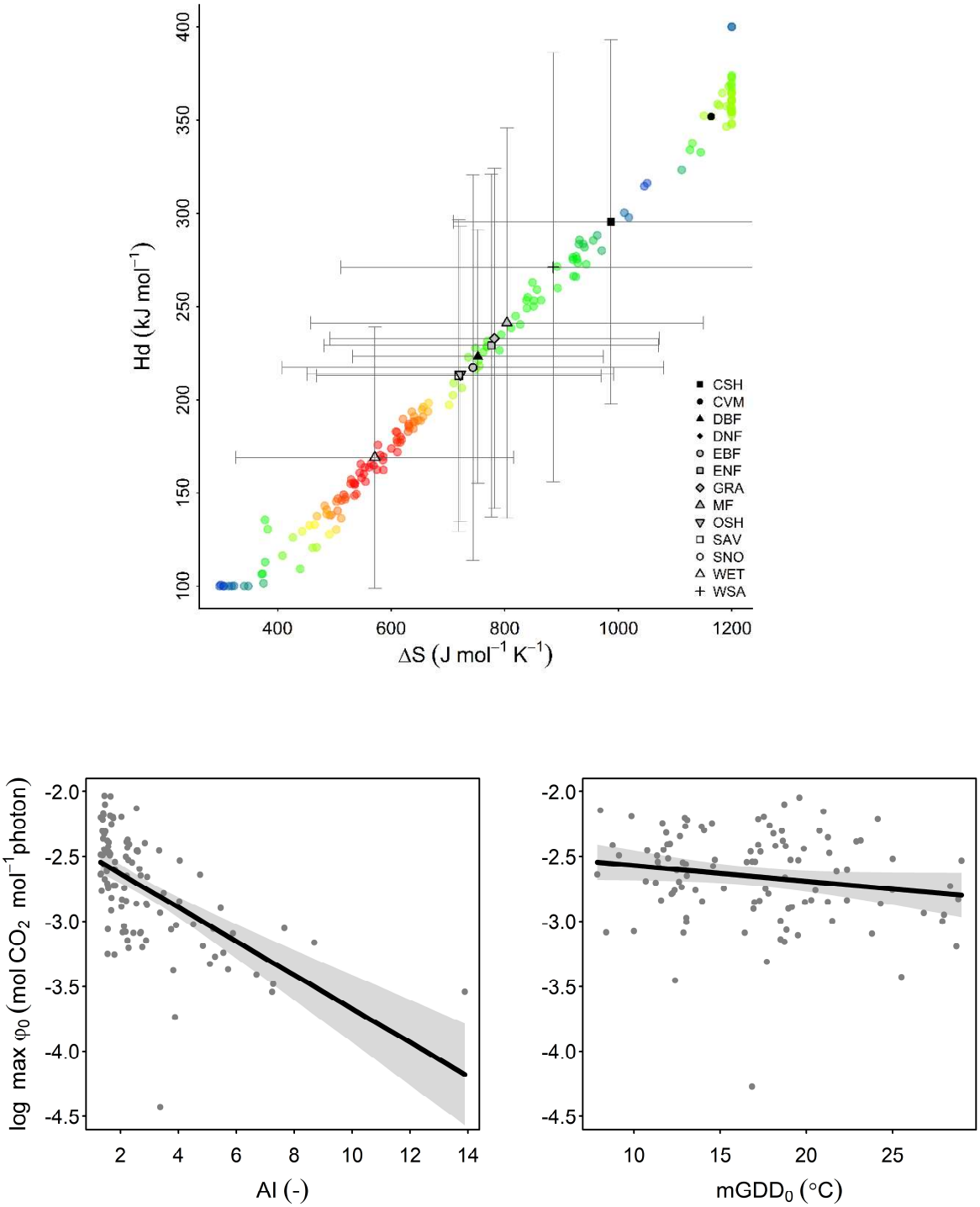

Figure A3. Other patterns in the PA parameters. **a** activation entropy and deactivation energy. **b** partial residual plot of $\widehat{\varphi_0}$ and AI. **c** partial residual plot of $\widehat{\varphi_0}$ and $mGDD_0$.

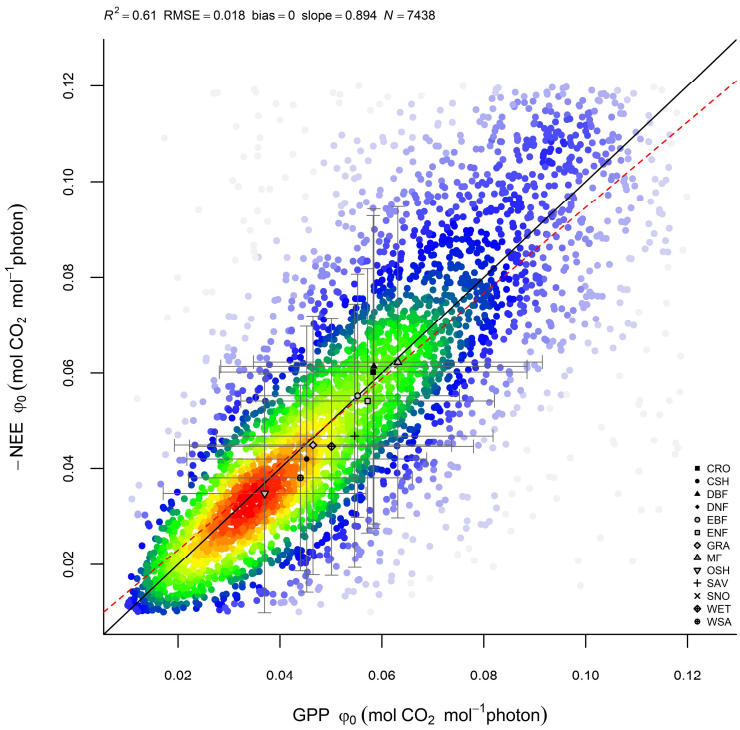

Figure A4. Correlation of estimated φ_0 with NEE and estimated with GPP using the FLUXNET dataset.

References

1. Harrison, S. P. *et al. Eco‐evolutionary optimality as a means to improve vegetation and land‐surface models*. *New Phytologist* (2021). doi:10.1111/nph.17558.
2. Rogers, A. *et al.* A roadmap for improving the representation of photosynthesis in Earth system models. *New Phytol.* **213**, 22–42 (2017).
3. Prentice, I. C., Liang, X., Medlyn, B. E. & Wang, Y.-P. Reliable, robust and realistic: the three R's of next-generation land-surface modelling. *Atmos. Chem. Phys.* **15**, 5987–6005 (2015).
4. Dietze, M. C. Gaps in knowledge and data driving uncertainty in models of photosynthesis. *Photosynth. Res.* **119**, 3–14 (2014).
5. Long, S. P., Postl, W. F. & Bolhár-Nordenkampf, H. R. Quantum yields for uptake of carbon dioxide in C3 vascular plants of contrasting habitats and taxonomic groupings. *Planta* **189**, 226–234 (1993).
6. Emerson, R. The Quantum Yield of Photosynthesis. *Annu. Rev. Plant Physiol.* **9**, 1–24 (1958).
7. Warburg, O., Burk, D., Schocken, V. & Hendricks, S. B. The quantum efficiency of photosynthesis. *Biochim. Biophys. Acta* **4**, 335–348 (1950).
8. Hill, J. F. & Govindjee. The controversy over the minimum quantum requirement for oxygen evolution. *Photosynth. Res.* **122**, 97–112 (2014).
9. Walker, D. Tansley Review No. 36 Excited leaves. *New Phytol.* **121**, 325–345 (1992).
10. Ehleringer, J. & Björkman, O. Quantum Yields for CO2 Uptake in C3 and C4 Plants. *Plant Physiol.* **59**, 86–90 (1977).
11. Ehleringer, J. & Pearcy, R. W. Variation in Quantum Yield for CO2 Uptake among C3 and C4 Plants. *Plant Physiol.* **73**, 555–559 (1983).
12. Björkman, O. & Demmig, B. Photon yield of O2 evolution and chlorophyll fluorescence characteristics at 77 K among vascular plants of diverse origins. *Planta* **170**, 489–504 (1987).
13. Singsaas, E. L., Ort, D. R. & DeLucia, E. H. Variation in measured values of photosynthetic quantum yield in ecophysiological studies. *Oecologia* **128**, 15–23 (2001).
14. Skillman, J. B. Quantum yield variation across the three pathways of photosynthesis: Not yet out of the dark. *J. Exp. Bot.* **59**, 1647–1661 (2008).
15. Zhang, Y. *et al.* Coupled estimation of 500 m and 8-day resolution global evapotranspiration and gross primary production in 2002–2017. *Remote Sens. Environ.* **222**, 165–182 (2019).

16. Bao, S. *et al.* Environment-sensitivity functions for gross primary productivity in light use efficiency models. *Agric. For. Meteorol.* **312**, (2022).
17. Cao, J. J. *et al.* Leaf hydraulics coordinated with leaf economics and leaf size in mangrove species along a salinity gradient. *Plant Divers.* (2022) doi:10.1016/j.pld.2022.01.002.
18. Farquhar, G. D., von Caemmerer, S. & Berry, J. A. A biochemical model of photosynthetic CO2 assimilation in leaves of C3 species. *Planta* **149**, 78–90 (1980).
19. von Caemmerer, S. *Biochemical models of leaf photosynthesis*. (CSIRO, 2000).
20. Rogers, A., Serbin, S. P., Ely, K. S. & Wullschleger, S. D. Terrestrial biosphere models may overestimate Arctic CO2 assimilation if they do not account for decreased quantum yield and convexity at low temperature. *New Phytol.* **223**, 167–179 (2019).
21. Bloomfield, K. J., Stocker, B. D., Keenan, T. F. & Prentice, I. C. Environmental controls on the light use efficiency of terrestrial gross primary production. *Glob. Chang. Biol.* **29**, 1037–1053 (2023).
22. Genty, B., Briantais, J. M. & Baker, N. R. The relationship between the quantum yield of photosynthetic electron transport and quenching of chlorophyll fluorescence. *Biochim. Biophys. Acta - Gen. Subj.* **990**, 87–92 (1989).
23. Bernacchi, C. J., Pimentel, C. & Long, S. P. In vivo temperature response functions of parameters required to model RuBP-limited photosynthesis. *Plant, Cell Environ.* **26**, 1419–1430 (2003).
24. Yin, X., Belay, D. W., Van Der Putten, P. E. L. & Struik, P. C. Accounting for the decrease of photosystem photochemical efficiency with increasing irradiance to estimate quantum yield of leaf photosynthesis. *Photosynth. Res.* **122**, 323–335 (2014).
25. June, T., Evans, J. R. & Farquhar, G. D. A simple new equation for the reversible temperature dependence of photosynthetic electron transport: a study on soybean leaf. *Funct. Plant Biol.* **31**, 275 (2004).
26. Dwyer, S. A., Ghannoum, O., Nicotra, A. & Von Caemmerer, S. High temperature acclimation of C 4 photosynthesis is linked to changes in photosynthetic biochemistry. *Plant, Cell Environ.* **30**, 53–66 (2007).
27. Zhang, L.-M. *et al.* Seasonal variations of ecosystem apparent quantum yield (α) and maximum photosynthesis rate (Pmax) of different forest ecosystems in China. *Agric. For. Meteorol.* **137**, 176–187 (2006).
28. Bibi, A. C., Oosterhuis, D. M. & Gonias, E. D. Molecular biology amd physiology: Photosynthesis, quantum yield of photosystem II and membrane leakage as affected by high temperatures in cotton genotypes. *J. Cotton Sci.* **12**, 150–159 (2008).
29. Novick, K. A. *et al.* The AmeriFlux network: A coalition of the willing. *Agric. For. Meteorol.* **249**, 444–456 (2018).

30. Prentice, I. C., Dong, N., Gleason, S. M., Maire, V. & Wright, I. J. Balancing the costs of carbon gain and water transport: Testing a new theoretical framework for plant functional ecology. *Ecol. Lett.* **17**, 82–91 (2014).
31. Stocker, B. D. *et al.* P-model v1.0: an optimality-based light use efficiency model for simulating ecosystem gross primary production. *Geosci. Model Dev.* **13**, 1545–1581 (2020).
32. Pastorello, G. *et al.* The FLUXNET2015 dataset and the ONEFlux processing pipeline for eddy covariance data. *Sci. Data* **7**, 225 (2020).
33. Myneni, R. B., Knyazikhin, Y. & Park, T. MCD15A3H MODIS/Terra+Aqua Leaf Area Index/FPAR 4-day L4 Global 500m SIN Grid V006 [Data set]. at https://doi.org/10.5067/MODIS/MCD15A3H.006 (2015).
34. Long, S. P., Humphries, S. & Falkowski, P. G. Photoinhibition of Photosynthesis in Nature. *Annu. Rev. Plant Physiol. Plant Mol. Biol.* **45**, 633–662 (1994).
35. Sonoike, K. The different roles of chilling temperatures in the photoinhibition of photosystem I and photosystem II. *J. Photochem. Photobiol. B Biol.* **48**, 136–141 (1999).
36. Oberhuber, W. & Edwards, G. E. Temperature dependence of the linkage of quantum yield of photosystem II to CO2 fixation in C4 and C3 plants. *Plant Physiol.* **101**, 507–512 (1993).
37. Berry, J. A. & Bjorkman, O. Photosynthetic Response and Adaptation to Temperature in Higher Plants. *Annu. Rev. Plant Physiol.* **31**, 491–543 (1980).
38. Greer, D. H., Berry, J. A. & Björkman, O. Photoinhibition of photosynthesis in intact bean leaves: role of light and temperature, and requirement for chloroplast-protein synthesis during recovery. *Planta* **168**, 253–260 (1986).
39. Mattila, H. *et al.* Effects of low temperature on photoinhibition and singlet oxygen production in four natural accessions of Arabidopsis. *Planta* **252**, 1–17 (2020).
40. Tyystjärvi, E. & Aro, E. M. The rate constant of photoinhibition, measured in lincomycin-treated leaves, is directly proportional to light intensity. *PNAS* **93**, 2213–2218 (1996).
41. Osmond, C. B. What is photoinhibition? Some insights from comparisons of shade and sun plants. in *Photoinhibition: Molecular Mechanisms to the Field* (eds. Baker, N. & Bowyer, J.) 1–24 (Bios Scientific Publications, 1994).
42. Murata, N., Takahashi, S., Nishiyama, Y. & Allakhverdiev, S. I. Photoinhibition of photosystem II under environmental stress. *Biochim. Biophys. Acta - Bioenerg.* **1767**, 414–421 (2007).
43. Sage, R. F. & Kubien, D. S. The temperature response of C 3 and C 4 photosynthesis. *Plant. Cell Environ.* **30**, 1086–1106 (2007).
44. Demmig-Adams, B., Winter, K., Krüger, A. & Czygan, F.-C. Zeaxanthin and the

Induction and Relaxation Kinetics of the Dissipation of Excess Excitation Energy in Leaves in 2% O 2 , 0% CO 2. *Plant Physiol.* **90**, 887–893 (1989).

45. Johnson, J. E. & Berry, J. A. The role of Cytochrome b6f in the control of steady-state photosynthesis: a conceptual and quantitative model. *Photosynth. Res.* **148**, 101–136 (2021).

46. von Caemmerer, S. & Evans, J. R. Temperature responses of mesophyll conductance differ greatly between species. *Plant. Cell Environ.* **38**, 629–637 (2015).

47. Fu, Z. *et al.* Critical soil moisture thresholds of plant water stress in terrestrial ecosystems. *Sci. Adv.* **8**, 1–13 (2022).

48. Mengoli, G., Harrison, S. P. & Prentice, I. C. A global function of climatic aridity accounts for soil moisture stress on carbon assimilation. *Prepr. https//doi.org/10.5194/egusphere-2023-1261* (2023).

49. Hu, C., Elias, E., Nawrocki, W. J. & Croce, R. Drought affects both photosystems in Arabidopsis thaliana. *New Phytol.* **240**, 663–675 (2023).

50. Wright, I. J. *et al.* The worldwide leaf economics spectrum. *Nature* **428**, 821–827 (2004).

51. Valladares, F., Wright, S. J., Lasso, E., Kitajima, K. & Pearcy, R. W. Plastic Phenotypic Response to Light of 16 Congeneric Shrubs from a Panamanian Rainforest. *Ecology* **81**, 1925 (2000).

52. Adams, W. W., Smith, S. D. & Osmond, C. B. Photoinhibition of the CAM succulent Opuntia basilaris growing in Death Valley: evidence from 77K fluorescence and quantum yield. *Oecologia* **71**, 221–228 (1987).

53. Flo, V. *et al.* Climate and functional traits jointly mediate tree water-use strategies. *New Phytol.* **231**, 617–630 (2021).

54. Bassiouni, M., Manzoni, S. & Vico, G. Optimal plant water use strategies explain soil moisture variability. *Adv. Water Resour.* **173**, (2023).

55. Bachofen, C., Hülsmann, L., Revill, A., Buchmann, N. & D'Odorico, P. Accounting for foliar gradients in Vcmax and Jmax improves estimates of net CO2 exchange of forests. *Agric. For. Meteorol.* **314**, 108771 (2022).

56. Stevens, R. M., Ewenz, C. M., Grigson, G. & Conner, S. M. Water use by an irrigated almond orchard. *Irrig. Sci.* **30**, 189–200 (2011).

57. Ardo, J., Molder, M., El-Tahir, B. A. & Elkhidir, H. A. M. Seasonal variation of carbon fluxes in a sparse savanna in semi arid Sudan. *Carbon Balance Manag.* **3**, 7 (2008).

58. Kattge, J. & Knorr, W. Temperature acclimation in a biochemical model of photosynthesis: a reanalysis of data from 36 species. *Plant. Cell Environ.* **30**, 1176–1190 (2007).

59. Kumarathunge, D. P. *et al.* Acclimation and adaptation components of the temperature dependence of plant photosynthesis at the global scale. *New Phytol.* **222**, 768–784

(2019).

60. Busch, F., Hüner, N. P. A. & Ensminger, I. Increased air temperature during simulated autumn conditions does not increase photosynthetic carbon gain but affects the dissipation of excess energy in seedlings of the evergreen conifer jack pine. *Plant Physiol.* **143**, 1242–1251 (2007).

61. Medlyn, B. E. *et al.* Temperature response of parameters of a biochemically based model of photosynthesis. II. A review of experimental data. *Plant, Cell Environ.* **25**, 1167–1179 (2002).

62. Herrmann, H. A., Schwartz, J. M. & Johnson, G. N. From empirical to theoretical models of light response curves - linking photosynthetic and metabolic acclimation. *Photosynth. Res.* **145**, 5–14 (2020).

63. Smith, E. L. THE INFLUENCE OF LIGHT AND CARBON DIOXIDE ON PHOTOSYNTHESIS. *J. Gen. Physiol.* **20**, 807–830 (1937).

64. Tenhunen, J. D., Weber, J. A., Yocum, C. S. & Gates, D. M. Development of a photosynthesis model with an emphasis on ecological applications. II. Analysis of a data set describing the PM surface. *Oecologia* **26**, 101–119 (1976).

65. Carrara, A. *et al.* Radiation measurements at ICOS ecosystem stations. *Int. Agrophysics* **32**, 589–605 (2018).

66. Feister, U. & Grewe, R. Spectral albedo measurements in the UV and visible region over different types of surfaces. *Photochem. Photobiol.* **62**, 736–744 (1995).

67. Murphy, B. K. & Stinziano, J. R. A derivation error that affects carbon balance models exists in the current implementation of the modified Arrhenius function. *New Phytol.* **231**, 2371–2381 (2021).

68. Priestley, C. H. B. & Taylor, R. J. On the Assessment of Surface Heat Flux and Evaporation Using Large-Scale Parameters. *Mon. Weather Rev.* **100**, 81–92 (1972).

69. Yang, Y. & Roderick, M. L. Radiation, surface temperature and evaporation over wet surfaces. *Q. J. R. Meteorol. Soc.* **145**, 1118–1129 (2019).

Methods:

EC observations

We selected sites from the Ameriflux database which report measured fAPAR or photosynthetic photon flux density above and below the canopy, adding up to 53 sites covering several biomes, we used net ecosystem exchange (-NEE) since it is the actual quantity measured at the towers. We replicated our analysis using the 212 sites from the FLUXNET database using fAPAR from the MODIS MCD15A3 product [33] interpolated to daily timesteps to check whether the same patterns can be observed globally.

Control for absorbed light.

To estimate fAPAR from measured below canopy PPFD we used the following calculation [65]:

$$fAPAR = \frac{PPFD_{IN} - PPFD_{OUT} - PPFD_BC_{IN}(1 - \alpha_{soil})}{PPFD_{IN}} \qquad (4)$$

Where, $PPFD_{IN}$ is the incoming photosynthetic photon flux density at the top of the canopy, $PPFD_{OUT}$ is the outgoing photosynthetic photon flux density, $PPFD_BC_{IN}$ is the incoming photosynthetic photon flux density below the canopy. All PPFD measurements are in $\mu mol\, m^{-2} s^{-1}$. α_{soil} is the soil albedo in the visible region of the light spectrum, taken here as 0.17 from [66].

Then, the absorbed PPFD (I_{abs}) was estimated simply as PPFD*fAPAR.

Correction factor for photorespiration Γ* and vapour pressure deficit

In the low light region of the light response curve, the assimilation exhibits a linear response to light, we assumed here that the assimilation is limited only by the rate of ribulose-1,5-bisphosphate (RuBP)-regeneration:

$$A = \varphi_0 * I_{abs} * m_j \qquad (5)$$

Where the slope of the line $A \sim I_{abs}\, m_j$ is equal to φ_0. This slope is geometrically equal to φ_0 in equation (6):

$$A_{net} = A - R_d = \frac{\varphi_0\, I_{abs}\, m_j}{\sqrt{1+\left(\frac{\varphi_0\, I_{abs}\, m_j}{A_{sat}}\right)^2}} - R_d \qquad (6)$$

Here, the factor m_j was calculated using the least cost hypothesis [30,31] as follows:

$$m_j = \frac{c_i - \Gamma^*}{c_i + 2\Gamma^*} \approx \frac{c_a - \Gamma^*}{c_a + 2\Gamma^* + 3\Gamma^* \sqrt{\frac{1.6\,\eta^* D}{\beta(K+\Gamma^*)}}} \qquad (7)$$

Data analysis

We subset all the subdaily observations by temperature bins of 1.0 °C, starting from 0.0 °C to the maximum observed subdaily temperature. For each one of these subsets, we plotted I_{abs}*mj on the x-axis and -NEE on the y-axis. Then, to account for any other limitations such as soil moisture, we selected the upper envelope points of the point cloud using the 90% percentile and fit φ_0, A_{sat} and R_d from equation (6). We saved the φ_0 values per temperature bin per site.

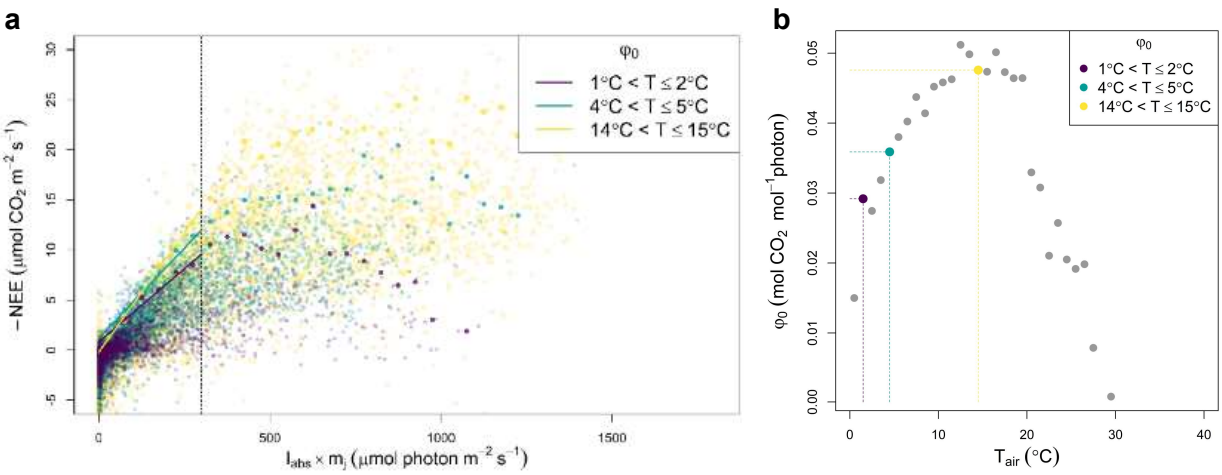

Figure 7. Method to extract $\varphi_0(T)$. Three 1.0 °C intervals with different colours are shown as an example for US-Bar (Biome: DBF, MAT=5.6 °C, MAP=1245 mm). **a** Light response curve at different temperatures. The upper envelope points (non-limited assimilation) here are shown bigger than the rest of the points. **b** φ_0 at different temperatures extracted from panel **a**.

Once φ_0 was found at each temperature bin, we fit $\varphi_0 = f(T)$ to a peak type Arrhenius equation [67] and repeated this procedure for all sites.

$$T_{opt} = \frac{H_d}{\Delta S - R\, log\left(\frac{H_a}{H_d - H_a}\right)} \qquad (8)$$

$$\varphi_0(T) = \widehat{\varphi_0}\left(\frac{T_{air}}{T_{opt}}\right)\exp\left(\frac{H_a\left(T_{air} - T_{opt}\right)}{R\, T_{opt}\, T_{air}}\right)\frac{1 + \exp\left(\frac{T_{opt}\,\Delta S - H_d}{R\, T_{opt}}\right)}{1 + \exp\left(\frac{T_{air}\,\Delta S - H_d}{R\, T_{air}}\right)} \qquad (9)$$

Bioclimatics

Aridity index was estimated as the ratio:

$$AI = \frac{PET}{P} \qquad (10)$$

Where PET is the mean annual potential evapotranspiration and P mean annual precipitation. Potential evapotranspiration was estimated following the Priestley Taylor model [68] with the corrections prosed by [69] to account for surface temperature feedback on the net radiation. While the actual evapotranspiration was estimated by converting the latent heat observed at the tower by the vaporization heat with corrections for local temperature and pressure.

Growing degree days (GDD_0) were estimated as number of days when air temperature > 0, while $mGDD_0$ was estimated as the average temperature during GDD.

Data availability

Code availability

References

Acknowledgements

Author contributions

Funding

Competing interests